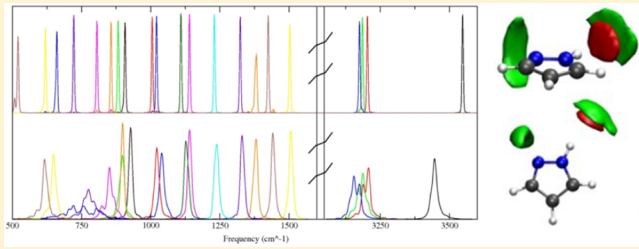


Vibrational Spectra of Water Solutions of Azoles from QM/MM Calculations: Effects of Solvation

Luana Tanzi,* Fabio Ramondo,* and Leonardo Guidoni*

Department of Physical and Chemical Sciences, University of L'Aquila, Via Vetoio, I-67100 L'Aquila, Italy

ABSTRACT: Using microsolvation models and mixed quantum/classical ab initio molecular dynamics simulations, we investigate the vibrational properties of two azoles in water solution: pyrazole and oxazole. The effects of the water-azole hydrogen bonding are rationalized by an extensive comparison between structural parameters and harmonic frequencies obtained by microsolvation models. Following the effective normal-mode analysis introduced by Martinez et al. [Martinez et al., *J. Chem. Phys.* 2006, 125, 144106], we identify the vibrational frequencies of the solutes using the decomposition of the vibrational density of states of the gas phase and solution dynamics. The calculated shifts from gas phase to solution are fairly in agreement with the available experimental data.



INTRODUCTION

Azoles are an important class of heteroaromatic molecules of biological interest. Their ability to form hydrogen bonding is due to the presence of donor groups, pyrrolic nitrogen (NH), and acceptor groups, pyridinic nitrogen. Such hydration sites give high solubility to these compounds in water and the determination of the structure of their aqueous solutions is a topic of great interest. The use of a combined approach, both theoretical and experimental, is, however, required in order to appropriately describe the structural and dynamical aspects of water solutions. X-ray as well as neutron diffraction are the main source of experimental information on the liquids structure, in particular on the solvent organization around solute. Alternatively, vibrational spectroscopy can be extremely useful to evaluate the effect of the environment on the solute structure following how vibrational properties of molecules change in presence of solvent.

The comparison between infrared (IR) or Raman spectra of isolated molecules (from gas phase or matrix isolation) and solution conditions can successfully indicate the role of the solvent in determining the structural properties of the solute. Such a comparative approach results particularly useful for molecules with vibrational modes quite easy to observe and assign in the different phases, as for example, carbonyl stretching. In these cases, the interpretation of the IR and Raman data can be carried out unambiguously and lead to the estimation of the effects of the solvent environment on the solute geometrical and electronic properties. Theoretical and computational approaches can be a valuable help for the understanding and the rationalization of these effects since they provide a direct correlation between structural and spectroscopic properties. In the present work, we apply quantum chemistry and ab initio molecular dynamics (AIMD) methods to investigate the solvation effect on the vibrational properties of a prototype of azole, pyrazole (see Figure 1a), a system

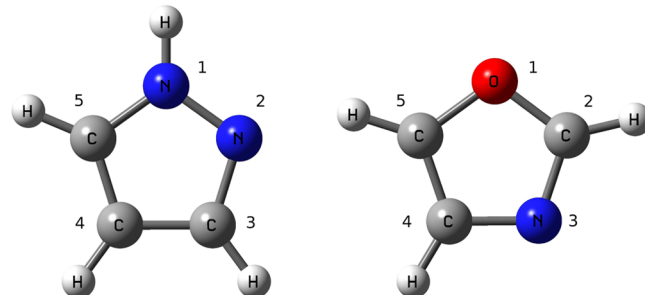


Figure 1. Numbering of atoms in pyrazole and oxazole.

already investigated by some of us through a combined X-ray diffraction and classical molecular dynamics (MD) study.¹ Gas phase quantum mechanics methods indicated that water molecules may surround pyrazole through NH···O and N···HO hydrogen bonds inducing significant changes in the geometrical and electronic structure of the molecule.¹ We expect therefore that also its vibrational properties could be sensitive to the solvent. Several experimental Raman and IR studies were reported for gas phase² water solution^{3–5} and solid state.^{3,6,7} Unfortunately, most studies do not show some bands very sensitive to the water environment, such as the NH stretching, because, in the same region, strong solvent absorptions are measured. Modes measured at lower frequencies are instead effectively affected by water solvent. The relatively high rigidity of the molecule excludes that the spectral differences observed from gas to liquid and solid phases can be caused by conformational changes. Moreover, pyrazole has two hydrogen bonding sites, one donor (NH) and one

Received: May 9, 2012

Revised: September 20, 2012

Published: September 24, 2012

acceptor (N), and it is interesting to study the effects of both the hydrogen bonds on the vibrational spectra, on the NH group vibrations, and on the ring modes. It is also intriguing to investigate how both intermolecular interactions can affect each other through the aromatic ring. For the sake of comparison, the present investigation is extended to another example of cyclic molecule, oxazole (Figure 1b), which has two acceptor groups (oxygen and nitrogen), and its spectral changes are limited to ring normal modes.⁸

The theoretical description of vibrational spectra in solution can be approached through different techniques and strategies. A simple approach is to consider microsolvation gas phase models, where one solute molecule is surrounded by a solvation shell of increasing numbers of solvent molecules to describe specific solvent–solute interactions occurring in solution. The relatively small size of such models allows to describe accurately the specific solute–solvent interactions at a quite high level of quantum mechanics (QM). By performing gas phase geometry optimization and normal-mode analysis, it is possible to selectively evaluate the effects of the solvent on each vibrational frequency and normal modes. This could be very useful to reveal cooperative or competitive effects due to multiple hydration as employed by some of us to elucidate the role of the solvent on the geometry and electronic properties of pyrazole in a previous study.¹ Similar microsolvation models are here proposed to investigate the effect of hydration on vibrational spectra of pyrazole and oxazole.

The microsolvation approach is representative of properties of gas phase cluster configuration at zero temperature and might not necessarily be representative of the real liquid system. More accurate descriptions of the solution should consider that solvation is a dynamic phenomenon, and therefore, the use of more appropriate theoretical approaches such as ab initio molecular dynamics should be taken into account. Using this technique, the temperature effect of the solution is explicitly considered, and IR and Raman spectra can be obtained from dipole and polarizability autocorrelation functions, respectively.⁹ In analogy to harmonic frequencies and normal-mode analysis, vibrational frequencies and effective normal modes can also be obtained from vibrational density of states (VDOS) decomposition, as displayed by the work of Martinez et al.¹⁰ Using this technique, dynamical solvation, temperature, and anharmonicity effects are directly and explicitly taken into account in the vibrational frequencies and normal modes.^{9,11}

AIMD are usually based on density functional theory (DFT) and can treat liquid systems with a relatively limited number of atoms. Quantum mechanics/molecular mechanics (QM/MM) simulations are a reasonable compromise to describe larger systems for simulating liquids and biomolecules.^{12–14} The solute molecule is treated at DFT level to correctly evaluate its vibrational properties, whereas the solvent is described through a classical force field. Taking into account the differences between the above cited techniques, vibrational and structural properties of pyrazole and oxazole in water solutions were here described using both microsolvation models and QM/MM simulations.

The article is organized as follows. In section 2, the computational details of the simulations are described. In section 3, first, the IR spectra of pyrazole and oxazole are discussed in the light of different microsolvation models. Then, frequencies of pyrazole and oxazole obtained from AIMD simulations are discussed for isolated and water molecules. Spectral changes obtained from theory are last compared with

IR spectra of both the molecules in different phases. Section 4 summarizes the conclusions.

COMPUTATIONAL DETAILS

Static Model Systems for Quantum Mechanics Study.

Quantum mechanical, static models were produced both for pyrazole and oxazole. For pyrazole, we proposed microsolvation models with an increasing number of water molecules (Figure 2), while for oxazole, we proposed three microsolvation models that underlined specific hydrogen bonding interactions (Figure 3).

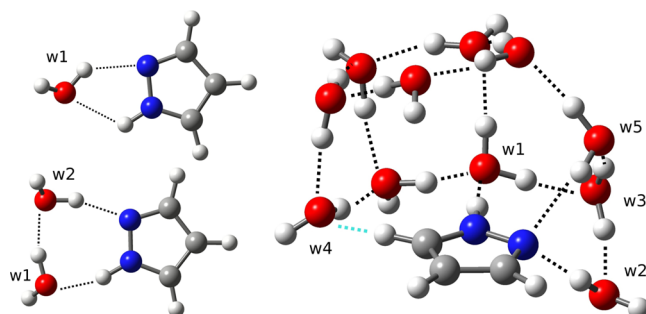


Figure 2. Pyrazole(H_2O) $_n$ microsolvation models with $n = 1, 11$.

DFT-based calculations were performed on isolated and hydrated molecules by the Gaussian03 package.¹⁵ Equilibrium structures and vibrational frequencies were obtained by analytical gradient based technique using the DFT, employing the B3LYP (Becke's three parameter exchange¹⁶ and Lee–Yang–Parr correlation¹⁷ potentials), combined with the 6-311++G** Gaussian basis set. Several pyrazole microsolvation models were previously studied¹ at this level since such this functional provides a description reasonably accurate of intermolecular interactions.¹⁸ Similar results were obtained using Perdew and Wang's exchange and correlation functionals (PW91),¹⁹ which partly recover dispersion interaction lost with the B3LYP method.²⁰ Anharmonic corrections were also included for pyrazole from third and semidiagonal fourth derivatives of energy following the procedure implemented in the Gaussian program.²¹

QM/MM simulations proposed in this work are based on a QM force field defined again on DFT methods; however, the DFT levels employed in the two approaches adopt different functionals and basis sets. For a more homogeneous comparison, we studied isolated molecules and some microsolvated structures with three different levels of theory: B3LYP/6-311++G**, PBE/6311++G**, and PBE/PW (70 Ry).

For the level PBE/PW (70 Ry), we employed the CPMD code,²² and potential energy calculations were carried out using exchange and correlation functionals proposed by Perdew, Burke, and Ernzerhof (PBE)²³ and a plane wave (PW) basis set. Plane waves expansion was developed in a periodic cubic system with unit cell edge of 21 au (about 11.1 ensemble) and truncated at 70 Ry. Pseudopotential functions were obtained employing Kleinman–Bylander scheme²⁴ along with norm-preserving Martins–Trouiller pseudopotentials.²⁵

Isolated molecules of pyrazole and oxazole were first described at all three levels. Specific solute–solvent interactions were then modeled using some of the microsolvation models previously proposed¹ focusing their attention on the B3LYP/6-

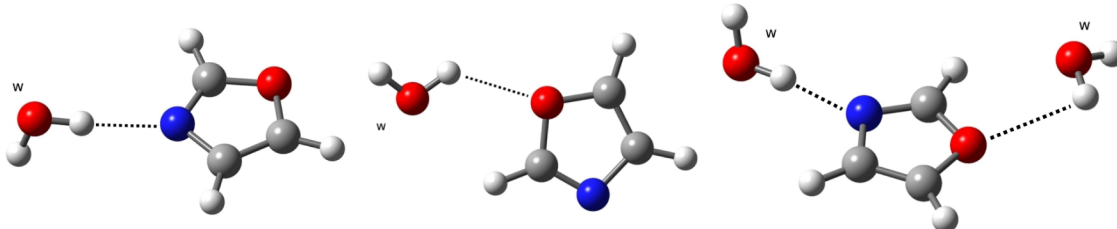


Figure 3. Oxazole microsolvation models: oxazoleN(H_2O), oxazoleO(H_2O), and oxazole(H_2O)₂.

31++G** vibrational frequencies. Effects of the theoretical level were evaluated by comparing the PBE/PW (70 Ry) and B3LYP/6-311++G** results for pyrazole(H_2O)₂. Implicit solvent calculations were further carried out using the polarizable continuum model (PCM).²⁶ As concerning oxazole, we proposed two models in which one water molecule selectively interacts at one hydration site: oxygen in oxazoleO(H_2O) or nitrogen in oxazoleN(H_2O). A third model was further investigated where oxazole simultaneously interacts with two water molecules, oxazole(H_2O)₂. All oxazole microsolvation models were studied at the B3LYP/6-311++G** level.

Model Systems for AIMD Study. Molecular dynamics simulations were performed both for isolated molecules (PYR, OXA) and for aqueous solution systems (PYRWAT, OXAWAT) using the CPMD code.²²

Isolated Molecules. Isolated molecules of pyrazole and oxazole were studied by Born–Oppenheimer molecular dynamics method (BOMD). Potential energy calculations were carried out with the same setup used for the level PBE/PW (70 Ry). Each system was equilibrated for 6.35 ps in the NVT ensemble at 20 K using the Nosé–Hoover thermostat.^{27–29} Each trajectory was collected (saving the coordinate every step) for 30 ps with a time step of 15 au (0.3627 fs) in the NVE ensemble. For every step, the total momentum and the global angular momentum of the PYR (or OXA) system were removed. Further simulations were repeated at 300 K to estimate the effect of temperature on the vibrational spectra of isolated molecules.

Molecules in Solution. PYRWAT and OXAWAT were studied by a mixed QM/MM method in which solute was described quantum-mechanically and solvent classically. Aqueous solution systems were built by xLeap, a program of the Amber8 package.³⁰ PYRWAT consists of 1 pyrazole molecule within a solvation box of 3076 rigid TIP3P³¹ water molecules, whereas OXAWAT consists of 1 oxazole molecule within a solvation box of 2835 rigid TIP3P³¹ water molecules. Pyrazole and oxazole were described using the general Amber force field (GAFF)³² using the atomic charges obtained by the AM1-BCC method.³³ Pyrazole and oxazole force fields were useful during classical pre-equilibration processes in which systems were simulated classically both in NPT and NVT ensembles using the Nosé–Hoover thermostat^{27–29} set at 300 K and the Parrinello–Rahman barostat^{34–36} set at 1 atm. Classical pre-equilibration processes, carried out with GROMACS 4.0.7 package,³⁷ were 400 ps long.

At the end of classical pre-equilibration processes, PYRWAT and OXAWAT were ready for QM/MM simulations. Solute was treated by BOMD using the same setup of the isolated systems without, however, removing the total momentum and the global angular momentum, whereas solvent was treated by classical molecular dynamics.

A multilayer approach was employed to deal with QM/MM electrostatic interaction.^{38,39} The first layer, defined as the classical water molecules within 8.5 Å from quantum atoms of the solute, screened the Coulomb terms between the electronic density and the classical point charges without any approximation. In the second layer, including classical atoms between 8.5 and 19 Å electrostatic interactions were computed using dynamically generated restrained electrostatic potential (D-RESP) derived charges fitted on the electronic density.³⁹ In the third layer, over 19 Å of electrostatic interactions were calculated using a multipolar expansion of the electron density.

A QM/MM equilibration in the NVT ensemble was done for 2.7 ps using a time step of 15 au and Nosé–Hoover thermostat set at 300 K. QM/MM trajectory was collected for 30 ps with a time step of 15 au in the NVE ensemble.

Moreover, we have evaluated the structural features of one microsolvation model, pyrazole(H_2O)₂, by dynamic descriptions at different levels. AIMD simulations were carried out at low (20 K) and room temperature (300 K) to estimate the effect of temperature on hydrogen bonded molecules. Simulations at 300 K were also carried out at the same QM/MM level applied for pyrazole in solution to compare QM and QM/MM results.

Vibrational Spectra and Assignment of Vibrational Modes. For quantum mechanics models, vibrational frequencies and normal modes were computed by diagonalization of the Hessian matrix of the potential energy surface (PES) at the equilibrium geometries. For AIMD models, vibrational frequencies of the solute were obtained by analyzing the VDOS:^{10,40}

$$\text{VDOS}(\omega) = \sum_{i=1}^N \int \left\langle \dot{r}_i(t) \dot{r}_i(0) \right\rangle \exp(i\omega t) dt \quad (1)$$

Since VDOS is defined as the sum of the Fourier transform of the atomic velocity autocorrelation functions (or power spectra), frequencies derived from such procedure include anharmonicity and temperature effects.⁴⁰ The VDOS spectra can be decomposed into the sum of power spectra of collective coordinates of the molecule q_k describing independent harmonic oscillations:^{10,40}

$$\text{VDOS}(\omega) = \sum_{k,l} \int \left\langle \dot{q}_k(t) \dot{q}_l(0) \right\rangle \exp(i\omega t) dt \quad (2)$$

The collective coordinates q_k are determined minimizing the functional $\Omega^{(n)}$:

Table 1. Main Structural Changes of Solute in Water and Equilibrium Geometry of Solute–Solvent Interactions from Static B3LYP/6-311++G** Microsolvation Models; PBE/PW(70 Ry) Shifts Are Reported in Parentheses

	pyrazole(H ₂ O)	pyrazole(H ₂ O) ₂	pyrazole(H ₂ O) ₁₁
ΔνNH (cm ⁻¹)	-80	-319 (-404)	-288
Δβ NH (cm ⁻¹)	17	41 (47)	42
ΔγNH (cm ⁻¹)	201	361 (374)	405
r(N2…Hw) (Å)	2.049	1.860	1.963/2.194
r(N1H1…Ow) (Å)	2.212	1.872	1.918
∠(N2…HOw) (deg)	135.0	160.2	167.9/157.0
∠(N1H1…Ow) (deg)	119.6	158.0	177.5
	oxazoleN(H ₂ O)	oxazoleO(H ₂ O)	oxazole(H ₂ O) ₂
Δβ CH (cm ⁻¹)	14	-15	5
ΔγCH (cm ⁻¹)		24	34
r(N3…Hw) (Å)	1.987		1.981
r(O1…Hw) (Å)		2.249	2.680
r(CH…Ow) (Å)		2.573	2.361
∠(N3…HOw) (deg)	174.6		175.2
∠(O1…HOw) (deg)		127.4	106.4

$$\Omega^{(n)} = \sum_k \left[\frac{\beta}{\pi} \int d\omega |\omega^{2n}| P_k^q(\omega) - \left(\frac{\beta}{2\pi} \int d\omega |\omega^n| P_k^q(\omega) \right)^2 \right] \quad (3)$$

where $P_k^q(\omega)$ is the power spectrum of k th collective coordinate q_k , and n is a fixed parameter, and imposing, as necessary conditions, the decorrelation of vibrational normal modes and the equipartitioning of the energy:

$$\begin{aligned} & \frac{1}{2\pi} \int d\omega \int \langle \dot{q}_k(t) \dot{q}_l(0) \rangle \times \exp(i\omega t) dt \\ &= \langle \dot{q}_k(t) \dot{q}_l(t) \rangle \\ &= k_B T \delta_{kl} \end{aligned} \quad (4)$$

The minimization of functional $\Omega^{(n)}$ leads to an eigenvalue problem providing effective normal modes. We carried out minimization setting $n = -1$. For each effective normal mode, the power spectrum becomes localized in frequency.^{10,40}

Properties Calculations. Analyzing the AIMD trajectories, mean geometries have been calculated as time average, and associated errors are estimated by including errors due to data correlation:

$$\sigma = \frac{\sqrt{\sum_{i=1}^N (d_i - \bar{d})^2}}{\sqrt{\frac{N}{\tau_c}}} \quad (5)$$

where \bar{d} is the mean value of the geometric parameter, N is the number of values d_i collected during dynamic every τ , and τ_c is the correlation time, expressed in units of and estimated by the autocorrelation function of $d(\tau)$. Structural informations on hydrogen bond interactions have been here analyzed by monitoring the N…O distance and the NH…O or N…OH angles following the criteria applied by the g-hbond tool of Gromacs.³⁷ To evaluate the numbers of water–solute interactions, cutoffs of 3.5 Å for N…O distances and 30° for HN…O and OH…N angles were assumed.

Associated errors to frequencies were estimated with the following procedure. Fractions of trajectory from the whole set

were selected, and vibrational frequencies were calculated for each portion with the procedure described above. The maximum fluctuations are predicted for those modes more involved by solvation, such as NH stretching; however, discrepancies were not higher than 5 cm⁻¹.

RESULTS AND DISCUSSION

Microsolvation Models. Pyrazole. Structures where pyrazole specifically interacts with a few water molecules are undoubtedly very useful to evaluate the role of every single interaction in the solvation process. With the aim to focus our attention on spectral changes caused by solvent, we carried out normal-mode analysis calculations on some geometry optimized structure of pyrazole microsolvation models previously described:¹ pyrazole(H₂O), pyrazole(H₂O)₂, and pyrazole(H₂O)₁₁ here reproduced in Figure 2. Pyrazole(H₂O) (Figure 2a) shows a water molecule interacting with both pyridinic and pyrrolic sites. Notwithstanding hydrogen bonds are very weak (long distances, N2…Hw1 = 2.049 Å and N1H1…Ow1 = 2.212 Å; angles far from linearity, ∠ N2…HOw1 = 135.0° and ∠ N1H…Ow = 119.6°), significant changes of the solute structure are predicted. Frequency shifts mainly occur at vibrational modes of the N1H group: red shift for N1H stretching, ΔνNH = -80 cm⁻¹, and blue shift for N1H bending modes both in plane, ΔβNH = 17 cm⁻¹, and out of plane, ΔγNH = 201 cm⁻¹. A second water molecule in pyrazole(H₂O)₂ allows the formation of a small hydrogen bond network, which connects, as a bridge, the pyrrolic to the pyridinic sites (Figure 2b). This network ensures more stable intermolecular interactions: shorter distances, N2…Hw2 = 1.860 Å and N1H1…Ow1 = 1.872 Å, and angles more close to linearity, ∠N2…HOw2 = 160.2° and ∠N1H…Ow1 = 158.0°. The hydrogen bonding effect on frequencies is consequently more evident: ΔνNH = -319 cm⁻¹, ΔβNH = 41 cm⁻¹, and ΔγNH = 361 cm⁻¹. When pyrazole(H₂O)₂ is calculated also at the level PBE/PW = 70 Ry, the theoretical model adopted for BOMD, frequencies are different from B3LYP/6-311++G** ones; however, the hydration shifts are again very similar revealing how these two levels of calculation estimate consistently solvent effects. Discrepancies are found only for νNH and γ ring modes at higher frequencies: their PBE/PW = 70 Ry shifts are higher than B3LYP/6-311++G** ones (see Table 1).

With the addition of more water molecules, the hydrogen bond network from pyridinic to pyrrolic sites increases its size and involves three water molecules; however, interactions gain indeed slightly in terms of stability. As previously observed,¹ pyrazole(H₂O)₁₁ (Figure 2c) shows a large hydration cage around pyrazole; the orientation of water allows the formation of an additional hydrogen bond at pyridinic site with water (w5 in Figure 2c: N2···Hw5 = 2.194 Å and \angle N2···HOw5 = 157.0°) and a dipolar interaction involving the CSH group and w4 (CH···Ow4 = 2.424 Å). Additional contacts at N2 weaken the interaction with w2 (N2···Hw2 = 1.963 Å and \angle N2···HOw2 = 167.9°). Hydration cage modifies the hydrogen bond at the pyrrolic site as well (N1H1···Ow1 = 1.918 Å and \angle N1H1···Ow1 = 177.5°) and affects the vibrational frequencies of the group NH: $\Delta\nu_{\text{NH}} = -288 \text{ cm}^{-1}$, $\Delta\beta_{\text{NH}} = 42 \text{ cm}^{-1}$, and $\Delta\gamma_{\text{NH}} = 405 \text{ cm}^{-1}$. The results summarized in Table 1 indicate that PBE/PW, the method used for quantum level of our QM/MM description of pyrazole in solution, and B3LYP/6-311++G** describe the hydration shifts in substantial agreement.

Oxazole. As for pyrazole, we studied preliminarily oxazole in water by building microsolvation models to identify the main interaction sites and evaluate the effects of specific oxazole–water interactions on solute structure: results are shown in Table 1. QM calculations indicate that the most energetic interaction site is N3 as witnessed by hydrogen bond with water in oxazoleN(H₂O) (Figure 3a). The comparison with the analogue pyrazole (H₂O) reveals that the intermolecular distance in oxazole is shorter (N3···Hw = 1.987 Å) and that the angle is closer to linearity (\angle N3···HOw = 174.6°). However, water in pyrazole(H₂O) lies between two nitrogen atoms, and thus, it interacts simultaneously with them through two different hydrogen bonds. Therefore, monohydration models do not allow to determine which pyridinic site is the best hydrogen bond acceptor between the two molecules. Most frequency shifts produced by a single water in oxazole are within 10 cm⁻¹. Only the CH bending at 1091 cm⁻¹ show appreciable shift of 14 cm⁻¹. As a matter of fact, the normal mode at 1091 cm⁻¹, identified as βCH , is significantly coupled with ring stretching coordinates, so hydration at N3 perturbs some ring internal coordinate and consequently βCH . The other hydration site of oxazole, O1, is an acceptor weaker than N3: oxazoleO (H₂O) (Figure 3b) presents, in fact, a O1···Hw (2.249 Å) hydrogen bond longer than N3···Hw and is very far from linearity (\angle O1···How = 127.4°). In such a complex, a second interaction involves the CH₂ group and water (H₂···Ow = 2.573 Å) suggesting the formation of a dipolar interaction. In conclusion, O1 hydration produces spectral changes very similar to those due to N3 hydration causing shifts on the CH bending at 1091 cm⁻¹ ($\Delta\beta\text{CH} = -15 \text{ cm}^{-1}$), which are appreciably coupled with ring internal coordinates. A new feature of O1 hydration is instead the fact that one γCH vibration, ($\gamma\text{CH} = 836 \text{ cm}^{-1}$) shifts by 24 cm⁻¹ as an effect of the dipolar interaction.

Oxazole(H₂O)₂ reported in Figure 3c describes the simultaneous hydration at both the atoms. QM geometries suggest that hydration at O1 does not affect that at N3: intermolecular structural features in oxazole (H₂O)₂ (N3···Hw = 1.981 Å and \angle N3···HOw = 175.2°) are very close to those in oxazoleN(H₂O). On the contrary, water at N3 affects the hydration structure at O1: water is now oriented to enhance dipolar interaction with CH₂ (H₂···Ow = 2.361 Å). Moreover water approaches O1 in oxazole(H₂O)₂ worse than in oxazoleO(H₂O) (O1···Hw = 2.680 Å). Consistently with

geometries, frequency shifts produced for oxazole(H₂O)₂ are practically the superposition of those observed in single hydrations at N3 and O1: βCH at 1091 cm⁻¹ increases only by 5 cm⁻¹ as a consequence of the opposite effects observed in the previous models, whereas the dipolar interaction at CH₂ changes the γCH frequency from 836 to 870 cm⁻¹. The double interaction on the ring heteroatoms produces a slight shift on the γCH frequency at 876 cm⁻¹ ($\Delta\gamma\text{CH} = 12 \text{ cm}^{-1}$).

Ab Initio Molecular Dynamics Results. Pyrazole in Vacuum at 20 and 300 K. Once discussed how water changes the solute structure by QM static hydration models, we analyze in this section the same effects by AIMD. Simulations have been carried out on pyrazole in water using QM/MM (PYRWAT simulation) and on pyrazole in vacuum (PYR) using the same DFT functional and basis set for both models. As a preliminary consideration, pyrazole was first simulated at low temperature (20 K) to easily compare the spectrum with that derived from equilibrium structure (Table 2). Frequencies were then obtained from 300 K simulations, and their values are reported in Table 3.

Table 2. Theoretical Frequencies (cm⁻¹) of Pyrazole in Gas Phase from QM and QM/MD Methods; Anharmonic Frequencies Are Reported in Parentheses

	B3LYP/6-311+ +G**	PBE/6-311+ +G**	PBE/PW (70 Ry)	VDOS PYR (20 K)
ν_{NH}	3665 (3499)	3580	3538	3548
ν_{CH}	3268 (3142)	3205	3198	3203
ν_{CH}	3251 (3117)	3187	3182	3185
ν_{CH}	3237 (3100)	3173	3170	3175
βCH	1563 (1528)	1513	1505	1503
βNH	1477 (1452)	1437	1423	1425
βCH	1420 (1385)	1391	1379	1382
βCH	1383 (1355)	1336	1327	1323
ν_{ring}	1279 (1256)	1240	1219	1230
ν_{ring}	1176 (1150)	1151	1141	1140
ν_{ring}	1141 (1114)	1118	1108	1109
ν_{ring}	1053 (1038)	1026	1022	1021
ν_{ring}	1046 (1014)	1020	997	1005
β ring	941 (928)	911	906	907
β ring	924 (912)	891	877	882
γCH	893 (883)	847	852	856
γCH	833 (836)	797	803	807
γCH	751 (746)	715	728	721
γ ring	687 (674)	670	626	659
γ ring	633 (624)	614	620	619
γNH	525 (532)	513	533	517

Before the discussion of spectral features, it is interesting to observe how mean geometries are affected by solvent environment. Figure 4 shows that PYR(20 K) mean geometry is indeed close to the equilibrium geometry calculated with the same functional, PBE. It means that vibrational motions are not critical in determining the mean geometry of the molecule and that this is expected for a rigid system like pyrazole. Notwithstanding the anharmonic corrections obtained by a second order perturbative treatment are not negligible for some modes like NH and CH stretching (see Table 2), the low temperature of simulations gives very similar medium and equilibrium geometries. However, mean geometry is not significantly changed also at room temperature, PYR (300 K), although the estimated errors on bond distances are higher.

Table 3. Theoretical and Experimental Frequencies (cm^{-1}) of Pyrazole in Gas Phase³ and Aqueous Solution³

	VDOS PYR(300 K)	VDOS PYRWAT(300 K)	IR vapor ³	Raman water solution ³
νNH	3539	3456	3523	
νCH	3179	3207–3188	3155	3150
νCH	3159	3187–3170	3137	3132
νCH	3153	3175–3154	3126	3119
βCH	1495	1507	1531	1538
βNH	1415	1442	1447	1476
βCH	1366	1381	1395	1399
βCH	1317	1329	1358	1356
νring	1223	1238	1254	1260
νring	1132	1141	1159	1151
νring	1103	1127	1121	1138
νring	1018	1040	1054	1050
νring	998	1022	1009	1038
$\beta\text{ ring}$	907	927	924	930
$\beta\text{ ring}$	886	898	908	915
γCH	852	898	879	867
γCH	803	852	833	834
γCH	720	775	745	772
$\gamma\text{ ring}$	647	649	674	657
$\gamma\text{ ring}$	612	617	623	612
γNH	500	803–756–720	516	

When PYR(20 K) geometry is compared with the experimental substitution geometry from microwave spectroscopy,⁴¹ a good approximation of the equilibrium structure, some deviations are found. By excluding systematic errors in experimental geometry, we think that the origin of this difference can be mainly due to the use of PBE functional since the B3LYP structure is closer to experiments.¹

Next, we analyze PYR(20 K) and PYR(300 K) frequencies (Tables 2 and 3). As expected, PYR(20 K) MD frequencies and harmonic frequencies calculated from equilibrium structure are indeed very similar (Table 2). PYR(300 K) frequencies reveals that temperature has a very small effect on the spectrum of isolated pyrazole since frequencies are lowered within 20 cm^{-1} at higher temperature. However, since hydration might produce spectral shifts of comparable amount, it is worth comparing PYR and PYRWAT both at room temperature (Table 3).

As concerning accuracy, we note that the PBE functional gives harmonic frequencies closer to experiment than B3LYP. When frequencies are derived from molecular dynamics, their values again well compare with QM harmonic frequencies, PBE/PW(70 Ry). Deviations from a vapor IR spectrum³ are indeed very small: NH and CH stretching frequencies are slightly higher, whereas the remaining modes are lower within 30 cm^{-1} . Since VDOS spectrum decomposition provides well localized effective normal modes with narrow peaks, we can

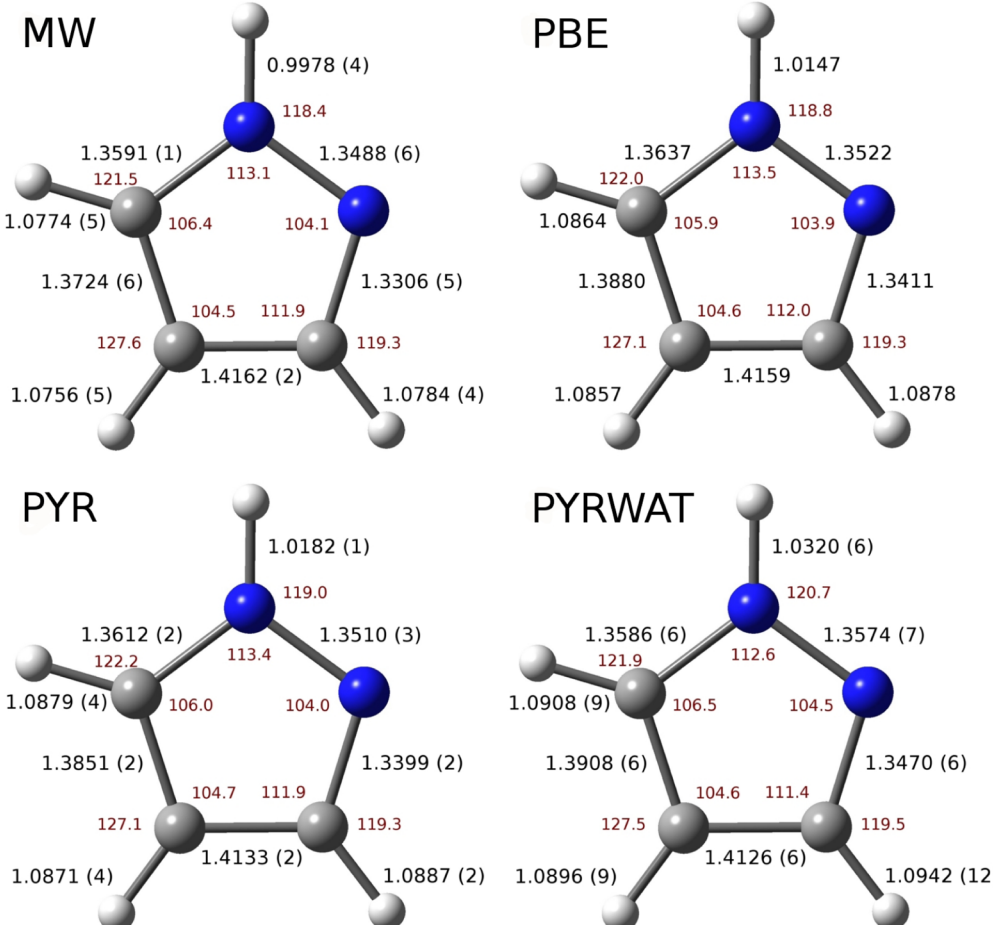


Figure 4. Substitution geometry from microwave spectroscopy⁴¹ (MW), equilibrium geometry from PBE/6-311++G** (PBE), and mean geometry from AIMD of isolated pyrazole (PYR). Mean geometry of pyrazole in water (PYRWAT) from QM/MM molecular dynamic (PYRWAT).

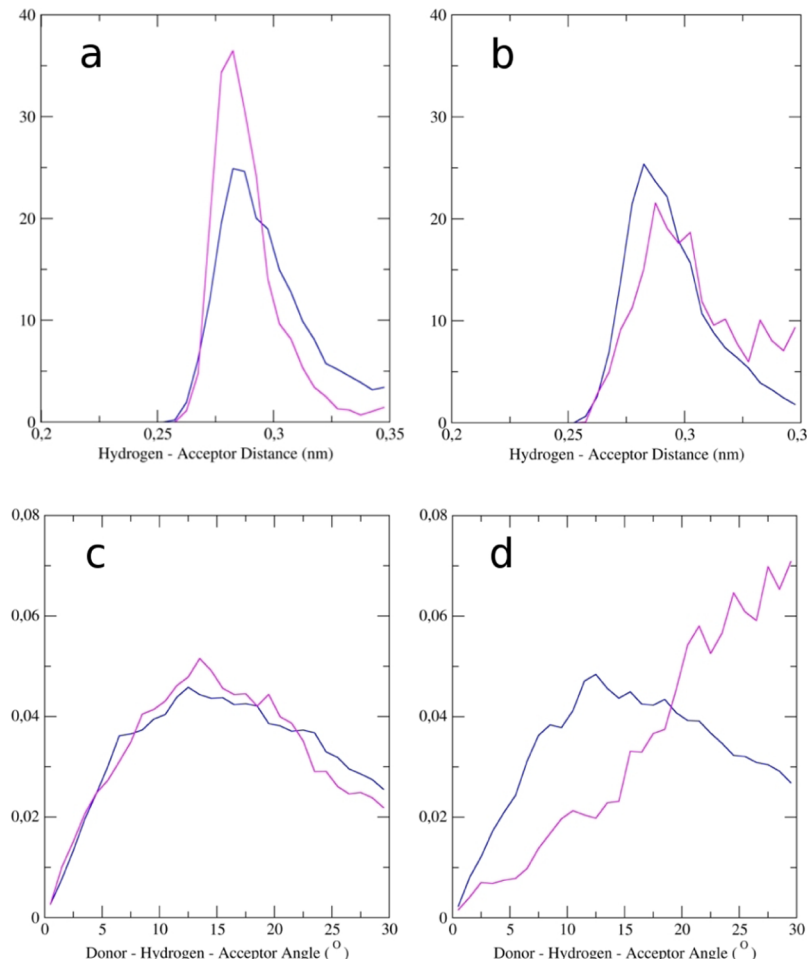


Figure 5. Distributions of hydrogen bond during AIMD dynamics of pyrazole in water, PYRWAT, and oxazole in water, OXAWAT. Pyrazole, distributions at N2 (blue) and N1H1 (red) for hydrogen bond distance (a) and hydrogen bond angle (c); oxazole, distributions at N3 (blue) and O1 (red) for hydrogen bond distance (b) and hydrogen bond angle (d).

attribute the small deviations from experimental data mainly to the DFT functional.

Pyrazole in Water. PYR and PYRWAT mean geometries reveal that solvent perturbs the solute structure in a qualitative agreement with the changes predicted from equilibrium structures of microsolvation models. Geometrical variations are mainly observed at the pyrrolic site, although small changes occur also at ring bond distances (Figure 4). Notwithstanding mean geometry of PYRWAT has errors larger than PYR, probably due to different simulation temperatures and to the presence of solvent environment, the structural perturbations are significant because within the estimated errors. On these grounds, we can conclude that solvation of pyrazole indeed changes its structure: the perturbations predicted from specific and static interactions are confirmed also when we include, more accurately, the possibility of hydrogen bond breaking and rearrangement.

The trajectory of PYRWAT simulations provides additional information on solvent environment. X-ray and MD previous studies showed that water coordinates the pyrrolic and pyridinic sites with a structure more peaked around the N pyrrolic group.¹ In agreement with the MD previous study, pyrrolic nitrogen is a single and strong hydrogen bond donor (Figure 5a), with a maximum N···O distance distribution at 2.82 Å. The pyridinic group has a hydrogen bond distance distribution more intense around a maximum again at 2.82 Å,

whereas bond angle distribution is broader (Figure 5b). Such differences in water structure have been rationalized by monitoring the number of hydrogen bonds during the simulations at both sites. Following these criteria, pyrrolic nitrogen forms most of the time a single hydrogen bond: the average number of hydrogen bonds (Nhb) is 0.9. Pyridinic nitrogen instead may form more often double hydrogen bond interactions (Nhb = 1.4), and this explains the more diffuse angular distribution of water molecules around this site (Figure 6).

Solvent dynamics at each site can be suggested by the residence time. The site was considered occupied if a water oxygen was found in a spherical volume with radius of 0.4 nm centered on N2 and N1, respectively. By fitting the resulting time function by an exponential,⁴² we calculated a residence time of 1.29 ps for the pyridinic site and 0.91 ps for the pyrrolic site. This is consistent with the fact that the stronger NH hydrogen bonding donor group may form one interaction, whereas N group may interact also doubly, as well witnessed by the average number of hydrogen bonds.

In agreement with the spectra of equilibrium microsolvation structures, dynamic descriptions of pyrazole in water predict spectral shifts more significant at the pyrrolic site, the NH stretching and out of plane NH bending modes (Table 3). Unfortunately, such bands are not reported in the Raman spectra of pyrazole in water;^{3–5} therefore, theoretical shifts are

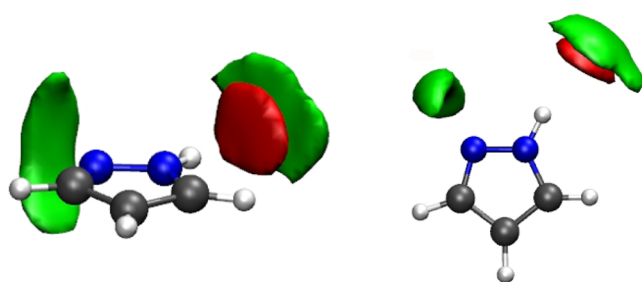


Figure 6. Spatial distribution functions of solvent hydrogens (green) and oxygen (red) in QM/MM simulation of pyrazole in water: two different views. The N2 site coordinates solvent hydrogens above and below the ring plane due to its behavior as a double acceptor of hydrogen bonding. The N1–water interactions mainly lie on the ring plane.

at present the only approach to evaluate the role of water on these vibrational properties. The alternative pyrazole microsolvation models, described in the previous section, predicted shifts on such modes that are different for each structure. The shifts predicted for pyrazole(H_2O)₂ and pyrazole(H_2O)₁₁, respectively, of -319 and -288 cm^{-1} are significantly larger than those obtained from the dynamic description (-83 cm^{-1}). These discrepancies are also observed when implicit solvent is included in the microsolvation framework (PCM) (-311 cm^{-1} for pyrazole(H_2O)₂ and -348 cm^{-1} for pyrazole(H_2O)₁₁).

Various factors could be responsible for the lack of agreement between the motionless clusters and the dynamic PYRWAT structure. First, the shifts derived from our solution simulations include the temperature effect (300 K), which allows dynamic descriptions of solvation, as well as anharmonicity, ignored at the equilibrium structure of microsolvation models. Second, notwithstanding pyrazole in cluster (QM) and in PYRWAT (QM/MM) is described by the same functional, the treatment of hydrogen bonding is different since in the QM/MM simulations with water are described in the MM region. As a matter of fact, a hydrogen bond crosses over the interface between the QM and MM regions, and electron reorganization is not taken into account. With the aim to factorize each contribution, molecular dynamics were carried out on pyrazole(H_2O)₂ with QM as well as QM/MM methods at different temperatures comparing the NH frequency shifts in Table 4.

An expected result is that QM(20 K) ν_{NH} frequency is quite close to the equilibrium (PBE/PW), whereas QM(300 K) simulations suggest that temperature has important effects on the hydrogen bonded molecules. Since we observed a modest temperature effect on isolated pyrazole, we can assign the change of ν_{NH} frequency shift from -410 cm^{-1} (20 K) to -300 cm^{-1} (300 K) to higher mobility of the hydrogen bond at room temperature. Notwithstanding distributions of hydrogen bonding in pyrazole solution indicate that pyrrolic group is a strong donor group, the mean intermolecular geometry $NH \cdots O$

of pyrazole(H_2O)₂ at 300 K, $1.92(10)\text{ \AA}$, is significantly higher than low temperature, $1.78(3)\text{ \AA}$, and equilibrium, 1.805 \AA , values. The first important conclusion is therefore that frequency shifts are affected by temperature and that dynamic descriptions should be always included also for simple gas phase hydrogen bonded cluster.

Table 4 also shows how in microsolvation models the spectral pattern due to hydration is affected by QM/MM method. Frequency shifts of NH modes of QM/MM pyrazole(H_2O)₂ are smaller, especially for ν_{NH} , than full QM values and are rather close to the QM/MM values in bulk solution (PYRWAT). This effect might be attributed to the lack of explicit polarization effects of the classical point charge water model whose force-field is obtained by fitting bulk properties. In conclusion, our QM/MM dynamic description of small hydrated complexes produce vibrational perturbations smaller than QM static approach for a combination of effects due to anharmonicity, temperature, and QM/MM methodology.

The last comparison in Table 4 between QM/MM pyrazole(H_2O)₂ and PYRWAT is again useful because this allows to estimate the effect of solvent beyond the first shell. The role of the solvent is significant because it further decreases the ν_{NH} shift (-83 cm^{-1}) and increases the β_{NH} shift. It is interesting to note that similar shift is found when the NH stretching in vapor pyrazole³ is compared with the NH stretching from IR spectrum of pyrazole solid,⁷ $\Delta\nu_{NH} = -98\text{ cm}^{-1}$, where molecules form strong $N \cdots HN$ hydrogen bonding.⁴³

There are other vibrational modes of pyrazole sensitive to the solvent, and their frequencies are measured both in vapor^{2,3} and in water solution.^{3–5} For example, the δ_{CH} bending undergoes a small blue shift (18 cm^{-1}) in agreement with the increase (29 cm^{-1}) observed from gas to solution spectra (Table 3). As for ν_{NH} stretching, PYRWAT and pyrazole(H_2O) shifts are very similar.

Most bands involving ring vibrations, ν_{ring} and β_{ring} , are predicted to increase their frequencies within about 20 cm^{-1} in agreement with the measured spectra. It means that our dynamic models of pyrazole describe satisfactorily the small spectral changes that solvent may cause on the ring modes. Higher blue shifts, within 50 cm^{-1} , are predicted for all three γ_{CH} modes. Since perturbations of γ_{CH} frequency are mainly originated by dipolar specific interactions between CH group and water, as pyrazole(H_2O)₁₁ suggests, displacements of all three γ_{CH} modes seem to indicate that solvation shell of pyrazole extends also to the whole region of the CH groups. In contrast with such results, only one γ_{CH} band, at 745 cm^{-1} , increases its frequency (27 cm^{-1}) in water. However, the origin of such discrepancies could be found in the fact that VDOS decomposition attests good localization in frequencies for all effective normal modes except for γ_{CH} and γ_{NH} modes (Figure 7).

Oxazole in Vacuum. As for pyrazole, vibrational motion affects only marginally the mean structural properties of

Table 4. Pyrazole NH Modes Frequency Shifts of Pyrazole(H_2O)₂ Microsolvation Model from Static (PBE/PW) and Dynamic (QM and QM/MM) Simulations at Different Temperatures; Comparison with PYRWAT (QM/MM in Bulk Water) Is Also Shown

	PBE/PW	QM(20 K)	QM(300 K)	QM/MM(300 K)	PYRWAT(300 K)
$\Delta\nu_{NH}\text{ (cm}^{-1}\text{)}$	-404	-410	-300	-114	-83
$\Delta\beta_{NH}\text{ (cm}^{-1}\text{)}$	41	48	32	22	27

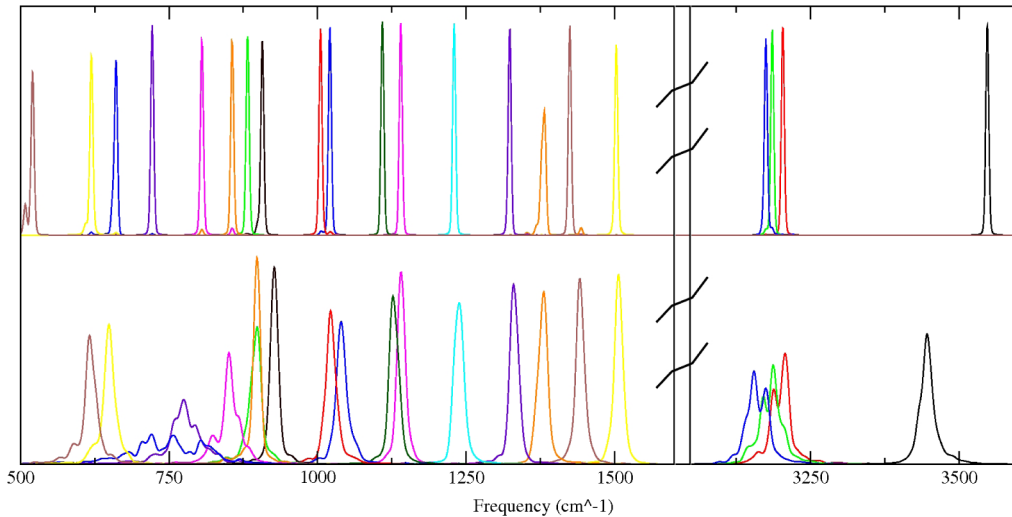


Figure 7. Power spectra of effective normal modes for pyrazole in vacuum (top) and in water (bottom) by decomposition of pyrazole VDOS.

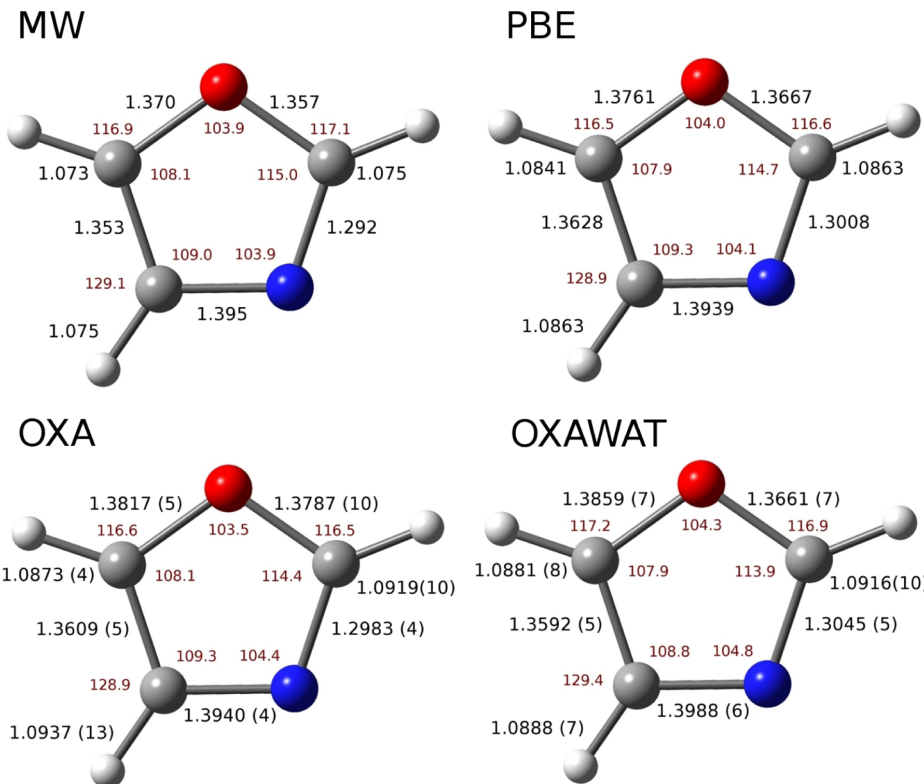


Figure 8. Oxazole geometric parameters by microwave spectroscopy⁴⁴ (MW), equilibrium geometry at the level PBE/6-311++G** (PBE), mean geometry of oxazole in vacuum obtained by ab initio molecular dynamic (OXA), and mean geometry of oxazole in water by QM/MM molecular dynamic (OXAWAT).

oxazole, and PBE/6-311++G** equilibrium structure (Figure 8b) and OXA mean structure (Figure 8c) are very similar. Some discrepancies are matched with the substitution geometry obtained by microwave spectroscopy⁴⁴ (Figure 8a), which can be mainly attributed to the PBE functional adopted in our calculations.

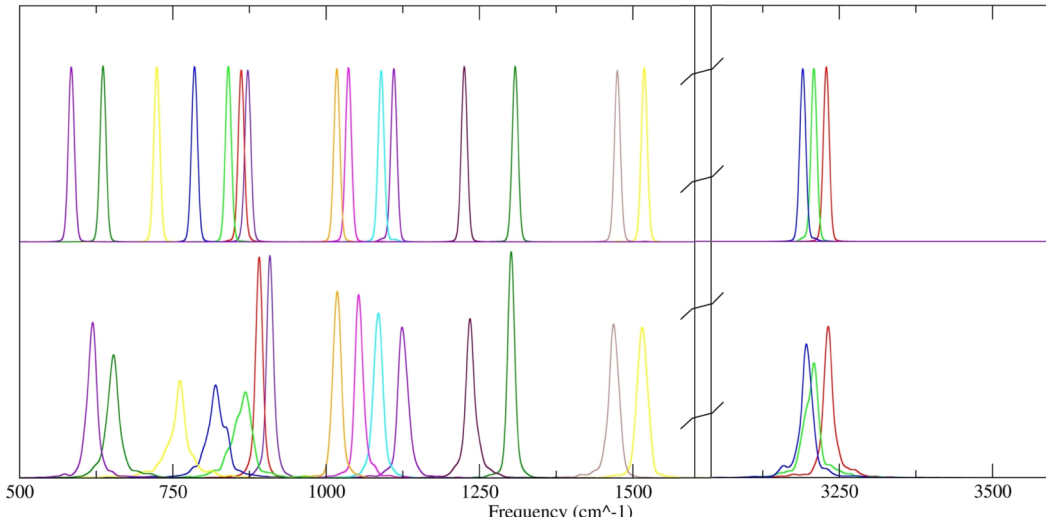
Table 5 shows harmonic frequencies from equilibrium structures and VDOS frequencies along with FTIR spectrum of oxazole in vapor.⁴⁵ VDOS spectrum presents narrow peaks, and effective normal modes are well localized in frequency (Figure 9). Theoretical results indicate that VDOS frequencies

do not significantly differ from harmonic ones, as already found for pyrazole.

Oxazole in Water. OXA and OXAWAT mean geometries suggest that solvation causes perturbations to the ring structure. Changes in distances and angles are substantially comparable with those observed in pyrazole; notwithstanding in oxazole, the two hydration sites are both hydrogen bond acceptors. However, the acceptor strengths of N3 and O1 are deeply different. Water distribution derived from OXAWAT indicates that O1 is a poor acceptor and that the number of its hydrogen bonds is so small that, most of the time, O1 is almost free from

Table 5. Theoretical and Experimental Frequencies (cm^{-1}) of Oxazole in Gas Phase^{45,47} and Aqueous Solution⁸

	B3LYP/6-311++G**	PBE/6-311++G**	PBE/PW(70 Ry)	VDOS OXA	VDOS OXAWAT	IR vapor ^{45,47}	Raman water solution ⁸
νCH	3296	3227	3222	3229	3231	3168	
νCH	3271	3205	3204	3208	3208	3148	
νCH	3258	3189	3184	3191	3196	3099	
νring	1574	1522	1520	1519	1514	1545	1551
νring	1524	1480	1474	1475	1469	1509	1510
νring	1355	1313	1309	1308	1302	1331	1334
βCH	1272	1224	1226	1225	1234	1260	1265
βCH	1159	1121	1106	1110	1124	1142	1156
νring	1118	1105	1090	1090	1085	1091	1094
βCH	1091	1053	1035	1036	1053	1081	
νring	1067	1043	1012	1017	1018	1052	1053
$\beta\text{ ring}$	929	896	870	872	908	909	927
$\beta\text{ ring}$	916	885	827	861	891	899	910
γCH	876	828	818	840	868	858	
γCH	836	783	773	785	819	832	
γCH	762	722	721	724	762	749	
$\gamma\text{ ring}$	661	645	621	636	653	646	
$\gamma\text{ ring}$	622	605	344	584	618	609	616

**Figure 9.** Power spectra of effective normal modes for oxazole in vacuum (top) and in water (bottom) obtained by decomposition of oxazole VDOS spectra.

water ($N_{\text{hb}} = 0.2$). The relative hydrogen bond distribution (Figure 5) is quite broad and without peaks, in agreement with a previous Car–Parinello MD study,⁴⁶ and no preferred orientation emerges from hydrogen bond angle distribution (Figure 5). As observed for pyrazole, N3 may act as double acceptor although single interactions are more probable during the collected trajectory. Pyridinic nitrogen in oxazole is a good acceptor as in pyrazole: its hydrogen bonds show a time average number of 1.3, a distance distribution with a maximum at 2.82–2.87 Å, and an angular distribution similar to that of pyrazole. VDOS effective normal mode decomposition of OXAWAT (Figure 9) shows well localized frequencies except for the γCH modes, as already found for pyrazole. If water changes the geometry of oxazole and pyrazole similarly, some important differences are found in the vibrational perturbations. In the high frequency region, the shifts are negligible since CH is not a hydrogen bonding donor. The ring vibrational modes are differently affected by solvent: νring are only marginally sensitive to water; this is in substantial agreement with the changes observed for these modes from vapor^{45,47} and to

solution^{8,46} spectra, $\beta\text{ ring}$ are instead a little overestimated by our models, increasing by about 30 cm^{-1} (Table 5). The lower blue shifts emerging for βCH from experiment are again reproduced by our VDOS spectra.

It is not straightforward to relate the spectral changes in this region to geometrical ring perturbation since νring , $\beta\text{ ring}$, and βCH modes are strongly coupled (Figure 10). However, the pattern of the ring vibrational shifts seems to indicate that breathing motions of the ring are the only modes sensitive to the solvent in oxazole. In pyrazole, instead, the molecule is involved more effectively in interactions with water, and this produces distortions also at bond distances.

Lastly, γCH modes are involved in important blue shifts, but unfortunately, no experimental data were reported in water solution spectra to evaluate the accuracy of the result.

CONCLUSIONS

This work reports a study on the effect of aqueous environment on vibrational properties of pyrazole and oxazole. Two different theoretical approaches have been employed to describe

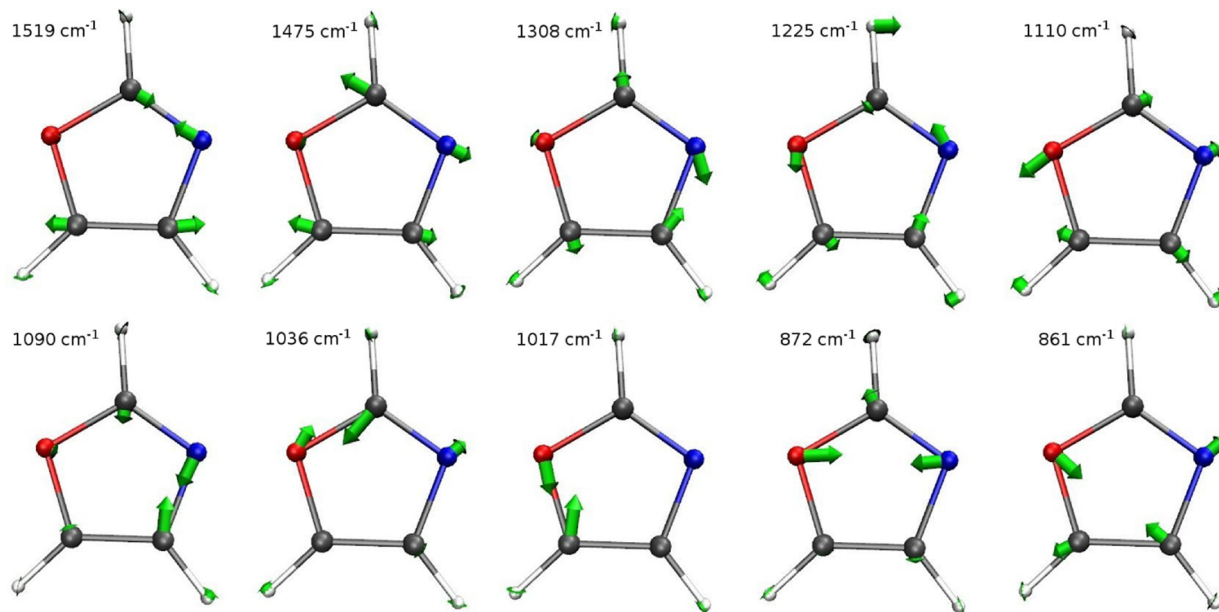


Figure 10. Effective normal modes ν_{ring} , β ring, and βCH of oxazole obtained from VDOS decomposition of oxazole in vacuum.

frequencies of the azoles in water solutions. Microsolvation models were first proposed to estimate the effect of specific interactions with solvent water molecules. From their static description, harmonic frequencies and normal modes were derived. One of these models, pyrazole(H_2O)₂, along with isolated pyrazole, was alternatively investigated by AIMD simulations at different temperatures, and frequencies were derived by using the VDOS decomposition. Dynamic models calculated vibrational shifts lower than static descriptions, revealing that temperature has an important role on the spectral perturbation due to hydration.

The effect of water solvent has then been estimated by QM/MM molecular dynamic simulations, and frequencies of solute were derived by using the VDOS decomposition introduced by Martinez et al.¹⁰ By attributing vibrational bands obtained from AIMD simulations to internal coordinates, it was possible to assign specific bands of isolated and solvated pyrazole and investigate in detail solvation effects on each band. In the case of pyrazole, AIMD simulations reveal that water coordination at two sites is different and that N2 lacks a sharp and preferred orientation of water with consequently higher mobility of the hydration shell with respect to the pyrrolic site. For the case of NH stretching of pyrazole, where no experimental information is available, our dynamical analysis shows a solvent shift of -83 cm^{-1} . Our QM/MM dynamic description of solvation produces vibrational perturbations smaller than the QM static approach for a combination of effects due to anharmonicity, temperature, and QM/MM methodology, indicating that effects of the solvation cannot be represented by single-point calculations.

The VDOS spectrum decomposition analysis provided overall well localized effective normal modes. The calculated frequency shift passing from gas phase to solution were in substantial agreement with that observed by vapor and solution spectra experiments. The solvent perturbation on the vibrational properties of oxazole was smaller since, in this case, only the nitrogen was significantly involved in hydration. Also in this case, the shift calculated by the gas phase and QM/MM simulations was in good agreement with the changes observed in the experiments.

■ AUTHOR INFORMATION

Corresponding Author

*E-mail: luana.tanzi@univaq.it (L.T.); fabio.ramondo@univaq.it (F.R.); leonardo.guidoni@univaq.it (L.G.).

Notes

The authors declare no competing financial interest.

■ ACKNOWLEDGMENTS

We acknowledge computational resources provided by CASPUR (grant std10-229). L.G. thanks CINECA for access to their computational facilities. L.T. thanks Dr. D. Bovi for the help and the technical support in the VDOS decomposition analysis.

■ REFERENCES

- (1) Ramondo, F.; Tanzi, L.; Campetella, M.; Gontrani, L.; Mancini, G.; Sadun, C. *Phys. Chem. Chem. Phys.* **2009**, *11*, 9431–9439.
- (2) King, S. T. *J. Phys. Chem.* **1970**, *74*, 2133–2138.
- (3) Majoube, M. *J. Raman Spectrosc.* **1989**, *20*, 49–60.
- (4) Muniz-Miranda, M.; Neto, N.; Sbrana, G. *J. Mol. Struct.* **1999**, *19*, 207–212.
- (5) Cardini, G.; Muniz-Miranda, M. *J. Phys. Chem.* **2002**, *106*, 6875–6880.
- (6) Durig, J. R.; Bergana, M. M.; Zunic, W. M. *J. Raman Spectrosc.* **1992**, *23*, 357–363.
- (7) Billes, F.; Endréi, H.; Jalovszky, G. *J. Mol. Struct.* **1999**, *465*, 157–172.
- (8) Muniz-Miranda, M. *Vib. Spectrosc.* **1999**, *19*, 227–232.
- (9) Gaigeot, M. P. *Phys. Chem. Chem. Phys.* **2010**, *12*, 3336–3359.
- (10) Martinez, M.; Gaigeot, M.-P.; Borgis, D.; Vuilleumier, R. *J. Chem. Phys.* **2006**, *125*, 144106–144114.
- (11) Spezia, R.; Bresson, C.; Auwer, C. D.; Gaigeot, M. P. *J. Phys. Chem. B* **2008**, *112*, 6490–6499.
- (12) Senn, H. M.; Thiel, W. *Angew. Chem., Int. Ed.* **2009**, *48*, 1198–1229.
- (13) Bovi, D.; Mezzetti, A.; Vuilleumier, R.; Gaigeot, M.-P.; Chazallon, B.; Spezia, R.; Guidoni, L. *Phys. Chem. Chem. Phys.* **2011**, *13*, 20954–20964.
- (14) Colombo, M.; Guidoni, L.; Laio, A.; Magistrato, A.; Maurer, P.; Piana, S.; Röhrig, U.; Spiegel, K.; Sulpizi, M.; VandeVondele, J.; Zumstein, M.; Röthlisberger, U. *Chimia* **2002**, *56*, 13–19.

- (15) Frisch, M. J.; et al. *Gaussian 03*, revision C.02; Gaussian Inc.: Wallingford CT, 2004.
- (16) Becke, A. D. *J. Chem. Phys.* **1993**, *98*, 5648–5652.
- (17) Lee, C.; Yang, W.; Parr, R. *Phys. Rev. B* **1988**, *37*, 785–789.
- (18) Rabuck, A. D.; Scuseria, G. *Theor. Chem. Acc.* **2000**, *104*, 439–444.
- (19) Perdew, J. P.; Chevary, J. A.; Vosko, S. H.; Jackson, K. A.; Pederson, M. R.; Singh, D. J.; Fiolhais, C. *Phys. Rev. B* **1992**, *46*, 6671–6687.
- (20) Tsuzuki, S.; Luthi, H. P. *J. Chem. Phys.* **2001**, *114*, 3949–3957.
- (21) Barone, V. *J. Chem. Phys.* **2005**, *122*, 1–10.
- (22) CPMD; IBM Corp. and Max Planck Institute: Stuttgart, Germany, 2012; see <http://www.cpmd.org/>.
- (23) Perdew, J. P.; Burke, K.; Ernzerhof, M. *Phys. Rev. Lett.* **1996**, *77*, 3865–3868.
- (24) Kleinman, L.; Bylander, D. M. *Phys. Rev. Lett.* **1982**, *48*, 1425–1428.
- (25) Troullier, N.; Martins, J. *Phys. Rev. B* **1991**, *43*, 1993–2006.
- (26) Cossi, M.; Barone, V.; Cammi, R.; Tomasi, J. *Chem. Phys. Lett.* **1996**, *255*, 327–335.
- (27) Nosé, S. *Chem. Phys.* **1984**, *81*, 511–519.
- (28) Nosé, S. *Mol. Phys.* **1984**, *52*, 255–268.
- (29) Hoover, W. G. *Phys. Rev. A* **1985**, *31*, 1695–1697.
- (30) Case, D. A.; et al. *AMBER 8*; University of California: San Francisco, CA, 2004.
- (31) Jorgensen, W. L.; Chandrasekhar, J.; Madura, J.; Klein, M. L. *J. Chem. Phys.* **1983**, *79*, 926–935.
- (32) Wang, J.; Wolf, R. M.; Caldwell, J. W.; Kollam, P. A.; Case, D. A. *J. Comput. Chem.* **2004**, *25*, 1157–1174.
- (33) Jakalian, A.; Bush, B. L.; Jack, D. B.; Bayly, C. I. *J. Comput. Chem.* **2000**, *21*, 132–146.
- (34) Parrinello, M.; Rahman, A. *Phys. Rev. Lett.* **1980**, *45*, 1196–1199.
- (35) Parrinello, M.; Rahman, A. *J. Appl. Phys.* **1981**, *52*, 7182–7190.
- (36) Martyna, G. J.; Tobias, D. J.; Klein, M. L. *J. Chem. Phys.* **1994**, *101*, 4177–4186.
- (37) Lindah, E.; Hess, B.; van der Spoel, D. *J. Mol. Model.* **2001**, *7*, 306–317.
- (38) Laio, A.; VandeVondele, J.; Rothlisberger, U. *J. Chem. Phys.* **2002**, *116*, 6941–6947.
- (39) Laio, A.; VandeVondele, J.; Rothlisberger, U. *J. Chem. Phys.* **2002**, *116*, 7300–7307.
- (40) Gaigeot, M.-P.; Martinez, M.; Vuilleumier, R. *Mol. Phys.* **2007**, *105*, 2857–2878.
- (41) Nygaard, L.; Christen, D.; Nielsen, J. T.; Pedersen, E. J.; Snerling, O.; Vestergaard, E.; Sorensen, G. O. *Mol. Struct.* **1974**, *22*, 401–413.
- (42) Impey, R. W.; Madden, P. A.; McDonald, I. R. *J. Phys. Chem.* **1983**, *87*, 5071–5083.
- (43) Foces-Foces, C.; Alkorta, I.; Elguero, J. *Acta Crystallogr., Sect. B: Struct. Sci.* **2000**, *S6*, 1018–1028.
- (44) Kumar, A.; Sheridan, J.; Stiefvater, O. L. Z. *Naturforsch.* **1978**, *33a*, 145.
- (45) Sbrana, G.; Castellucci, E.; Ginanneschi, M. *Spectrochim. Acta, Part A* **1967**, *23*, 751–758.
- (46) Pagliai, M.; Muniz-Miranda, M.; Cardini, G.; Schettino, V. *Phys. Chem. A* **2009**, *113*, 15198–15205.
- (47) Hegelund, F.; Larsen, R. W.; Palmer, M. H. *J. Mol. Spectrosc.* **2007**, *241*, 26–44.